(Received 7 May 2025, Accepted 4 July 2025, Scheduled 18 July 2025)

Development of a Compact Planar Antenna with Multi-Resonant Geometry for Broadband CubeSat Applications

Swati V. Yadav[1], Manish V. Yadav[2,*], and Dinesh Yadav[3,*]

[1]*Department of Instrumentation and Control Engineering, Manipal Institute of Technology Manipal Academy of Higher Education, Manipal, Karnataka 576104, India*
[2]*Department of Aeronautical and Automobile Engineering, Manipal Institute of Technology Manipal Academy of Higher Education, Manipal 576104, India*
[3]*Department of Electronics and Communication Engineering Manipal University Jaipur, Jaipur, Rajasthan, India*

ABSTRACT: This article presents the design and analysis of a Compact Planar Antenna with Multi-Resonant Geometry for Broadband CubeSat Applications. The antenna features a dual-layer architecture comprising a front semi-circular radiator with strategically positioned circular and rectangular slots, and a complex ground plane etched with complementary geometries to enhance performance. The optimized geometry, with key dimensions such as an overall size of 15 mm × 15 mm × 1.5 mm, enables a wide impedance bandwidth ranging from 2.9 GHz to 11.6 GHz. The impedance bandwidth of the radiator is 120%, with an electrical size of $0.14\lambda \times 0.14\lambda \times 0.014\lambda$. Confirmed through both simulation and measurement using a VNA in an anechoic chamber, the gain performance increases steadily with frequency, reaching a peak of 4.2 dBi at 9.2 GHz, while maintaining a stable gain above 3 dBi between 3.8 GHz and 10.1 GHz. Radiation efficiency peaks at 87% around 5.6 GHz and remains above 75% within the mid-band range (4–8 GHz), indicating highly effective power radiation and minimal losses. Surface current and 3D radiation pattern analysis show efficient and focused radiation behavior at 6 and 9 GHz, supporting its suitability for wideband radar and secure communication applications.

1. INTRODUCTION

The rapid growth in demand for high-speed wireless connectivity has driven significant progress in 5G and emerging 6G technologies. These future communication systems require antennas that are not only compact and efficient but also capable of operating across wide frequency spectrums with stable radiation patterns. Ultra-Wideband (UWB) antennas have gained attention for their suitability in multi-band applications, particularly in 5G networks, aerospace, and satellite communications. However, designing UWB antennas that offer wide impedance bandwidth while remaining small in size poses a major challenge. Traditional designs often compromise gain, complexity, or impedance matching.

This study proposes a compact UWB antenna that addresses these issues, offering enhanced bandwidth, gain, and efficiency. With dimensions of $15 \times 15 \times 1.5\,\text{mm}^3$, the antenna operates efficiently between 2.9 GHz and 11.6 GHz and a measured impedance bandwidth of 120%.

The rest of the paper is organized as follows. Section 2 reviews related work. Section 3 details the antenna design. Section 4 presents the simulation and measurement results, and Section 5 concludes with insights into future research directions.

* Corresponding authors: Manish Varun Yadav (yadav.manish@manipal.edu); Dinesh Yadav (dinesh.yadav@jaipur.manipal.edu).

2. RELATED WORK

Extensive research has been conducted to enhance UWB antenna performance for contemporary wireless systems. Various patch geometries such as U-shaped, semicircular, and rectangular microstrips have been widely investigated [1]. Performance enhancements have been realized through modifications like adding parasitic elements to the ground plane [2] and integrating fractal geometries or slots, which influence bandwidth and radiation characteristics [3].

Efforts to improve antennas for aeronautical communication have led to modified patch structures, such as incorporating flawed backsides and semicircular slots to widen bandwidth [4, 5]. Other studies have looked into flexible antennas with spherical or dumbbell-shaped designs [6, 13] and introducing cuts in the main patch to boost gain [7]. Past innovations also include incorporating semi-circular slots and ground structure defects to improve performance [10], while U-slot cuts have been used to achieve consistent polarized radiation [11]. Additionally, planar trapezoidal monopole antennas with coplanar waveguide (CPW) feed and notch features were introduced to mitigate interference in 3 and 3.5 GHz systems [12].

Antenna design has increasingly focused on sustainability and adaptability, especially for next-generation wireless systems. Notable advancements include the development of circularly polarized, multi-band UWB antennas fabricated on Rogers substrates, specifically tailored for wearable 5G/6G

technologies [14]. In the pursuit of advanced antenna solutions for modern communication systems, researchers have explored innovative designs that offer compactness, broad bandwidth, and multi-band capabilities. In 2019, Baudha et al. [15] presented a microstrip antenna with a dumbbell-shaped structure, demonstrating broadband performance ideal for space-constrained applications. More recently, Yadav et al. [16] developed a versatile antenna capable of operating across the S, C, and X bands, specifically aimed at supporting 5G and future wireless technologies. At millimeter-wave frequencies, such as 60 GHz, researchers have introduced sophisticated configurations like L-shaped stacked patches and phased array systems using high-density interconnect techniques to support high-performance communication [17]. Additionally, square-shaped patch antennas have shown potential in optimizing bandwidth and current flow for 5G use cases [18]. Collectively, these innovations reflect the continuous evolution in antenna engineering and highlight the increasing challenge of maintaining optimal impedance matching across broader frequency spectrums [19–21].

Reducing ground plane size has also proven effective in expanding frequency coverage, while design adjustments such as bending the radiating elements have been employed to focus signals more efficiently. For CubeSat and millimeter-wave systems, multiple-input multiple-output (MIMO) antenna development has advanced significantly. Sethi et al. [22] introduced a pattern diversity-based, dual-band, four-element MIMO patch antenna that minimizes signal fading and supports wideband operation. Munir et al. [23, 24] presented compact, wideband MIMO antennas optimized for vehicular and mmWave applications, addressing spatial and mobility constraints.

Metamaterial-inspired designs have further pushed the boundaries of miniaturization and bandwidth. Kukreja et al. [25, 26] proposed dual-band antennas using modified SRRs, interdigital capacitors, and U-shaped strips improve bandwidth, impedance matching, and radiation consistency. Core concepts in antenna and microwave engineering are extensively covered in the works of Balanis [27] and Pozar [28]. Balanis delivers detailed explanations on antenna design and theoretical analysis, whereas Pozar focuses on key aspects of microwave systems and components. These texts are widely regarded as fundamental resources for professionals and researchers working in these domains. Hexagonal patch geometries, chosen for their superior symmetry and broadside radiation traits, have shown promise in enhancing bandwidth, gain, and efficiency by reducing surface wave losses and promoting effective current flow [29–31]. Phase-change chalcogenide materials have emerged as key components for tunable photonic devices due to their reversible and fast switching properties. Cao et al. [32] demonstrated tunable thermal emission using a chalcogenide metasurface, enabling dynamic control of thermal radiation. Similarly, Cao et al. [33] reported ultrafast beam steering with plasmonic resonators based on Au-$Ge_2Sb_2Te_5$-Au, highlighting rapid optical modulation capabilities. These studies illustrate the potential of chalcogenide-based metasurfaces for actively reconfigurable optical applications. The growing demand for compact and efficient antennas in modern wireless systems has led to significant advancements in flexible and reconfigurable antenna designs. Soni et al. [34] proposed a flexible ring slot antenna optimized for 5G performance in the N77 and N78 bands, targeting wearable applications. Complementing this, Tiwari et al. [35] introduced a reconfigurable ultra-wideband circular monopole antenna with a wide notched band, using PIN diode switches to suppress interference. These developments highlight the potential of innovative antenna structures for next-generation communication systems.

2.1. Graphical Abstract Summary of the Proposed CubeSat Antenna

The graphical abstract, as shown in Figure 1, outlines the complete process of designing a compact antenna for CubeSat applications. It starts with a conceptual design, followed by electromagnetic simulations to analyze key performance parameters such as return loss (S_{11}), gain, and radiation patterns, ensuring optimal operation within the intended frequency range. The fabrication phase involves transferring the antenna pattern onto a substrate using photolithography and chemical etching with ferric chloride. Post-fabrication testing is conducted using a Vector Network Analyzer (VNA) inside an anechoic chamber to accurately measure the reflection coefficient and impedance. The final results, including measured S_{11} and radiation characteristics, confirm resonance at the desired frequency and directional behavior, closely matching simulation predictions and validating the antenna's effectiveness for CubeSat communication, as illustrated in Figure 1.

(A) **Simulation & Optimization**: This section features electromagnetic simulations, presenting key performance parameters such as return loss (S_{11}), gain, and radiation patterns. These results validate the antenna design against the operational frequency range and ensure optimized performance before fabrication.

(B) **Fabrication & Measurement**: The antenna is fabricated using a chemical etching process, where a pattern is transferred to the substrate using photolithography and etched using ferric chloride.

(C) Post-fabrication, the antenna's performance is tested using a VNA inside an anechoic chamber, allowing precise measurement of parameters such as reflection coefficient and impedance.

(D) **Results & Discussion**: This section presents the measured S_{11} (return loss) results, confirming resonance at the intended frequency, along with a radiation lobe diagram indicating the antenna's directional characteristics. The measured outcomes align closely with simulation predictions, validating the design's effectiveness for CubeSat communication applications.

3. ANTENNA DESIGN AND EVOLUTION

Figure 2 presents the front, side, and back views of a specially designed planar antenna structure for military applications, ac-

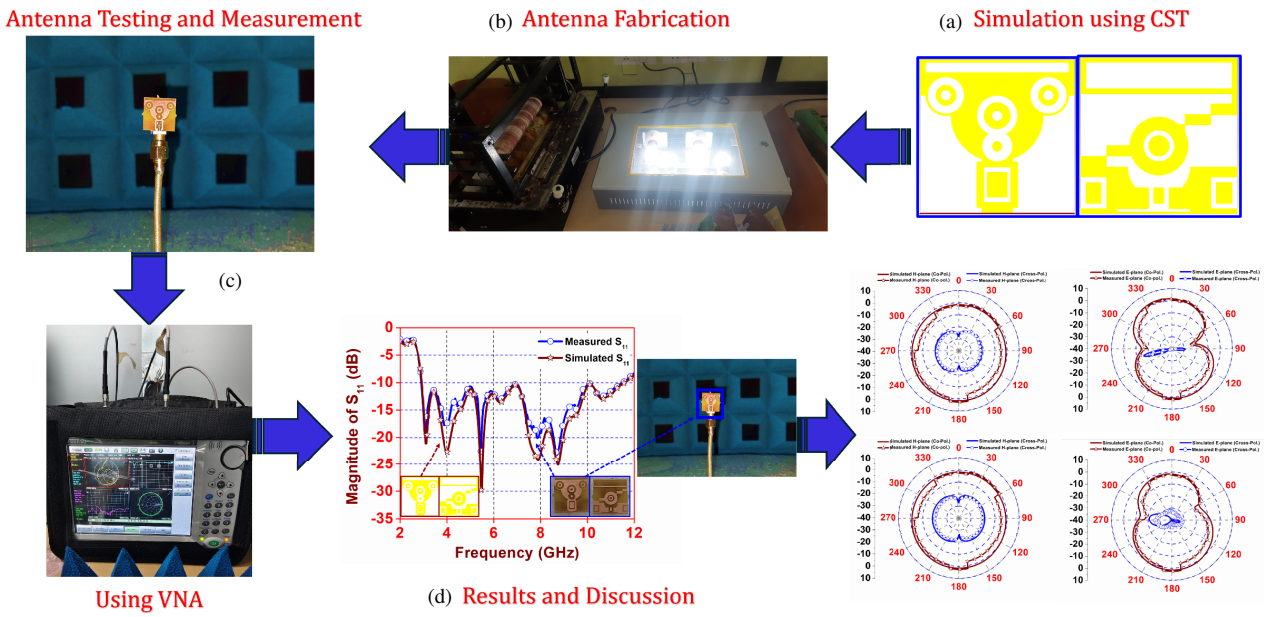

FIGURE 1. A graphic overview outlining the suggested methodology; (a) CST-based antenna simulation; (b) Antenna Lab fabrication unit representation. (c) Presents the constructed antenna design, testing, and measurement; (d) Offers a comparison between the results of simulation and measurement.

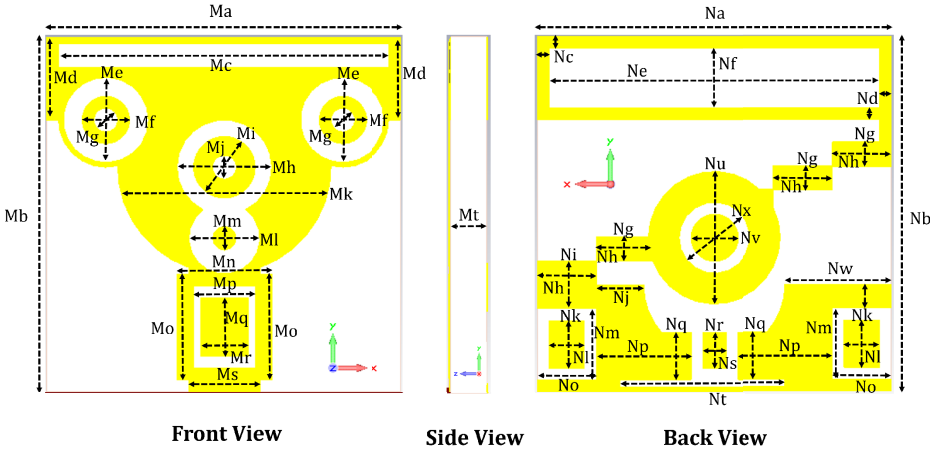

FIGURE 2. The configuration of the proposed CubeSat application.

companied by a detailed table (Table 1) specifying the geometric dimensions of various antenna components.

3.1. Geometrical Parameters of the Proposed Planar Antenna

(i) Antenna dimensions ($L \times W$): $15 \times 15\,\text{mm}^2$

(ii) Central patch width (Mc): 14 mm

(iii) Substrate thickness (Mt): 1.5 mm

(iv) Substrate material: Not specified (assumed typical high-frequency substrate)

(v) Patch width segments (Ma, Mb): 15 mm each

(vi) Feedline width (Mf): 2 mm

(vii) Feedline positioning parameter (Md): 3.5 mm

(viii) Circular segment diameters (Mj, Mi, Mk): 1 mm, 2.6 mm, 9 mm, respectively

(ix) Patch-ground gap (Me): 4 mm

(x) Ground plane width (Na): 15 mm

(xi) Ground plane height (Nb): 15 mm

(xii) Etched slot dimensions (Ne, Nf, Ng, Nd): 14 mm, 2.5 mm, 1 mm, 14 mm, respectively

(xiii) Circular back-side elements (Nx, Nv): 7 mm, 5.6 mm, respectively

(xiv) Ground plane positioning parameters (Nr, Ns, Nt): 4.5 mm, 1 mm, 7 mm, respectively.

TABLE 1. Geometry parameters of the special military application antenna.

Parameters	Ma	Me	Mb	Mf	Mc	Mg	Md	Mh	Mj
Values (mm)	15	4	15	2	14	1	3.5	4	1
Parameters	**Mi**	**Mo**	**Mk**	**Mp**	**Ml**	**Mq**	**Mm**	**Mr**	**Mn**
Values (mm)	2.6	4.5	9	2.6	3	2.5	1	2	4
Parameters	**Ms**	**Mt**	**Na**	**Ne**	**Nb**	**Nf**	**Nc**	**Ng**	**Nd**
Values (mm)	3	1.5	15	14	15	2.5	0.6	1	14
Parameters	**Nh**	**Nm**	**Ni**	**Nn**	**Nj**	**No**	**Nk**	**Np**	**Nl**
Values (mm)	2.5	3	2.03	2	2	2.5	2	4.1	1.5
Parameters	**Nq**	**Nv**	**Nr**	**Nw**	**Ns**	**Nx**	**Nt**	**Nu**	-
Values (mm)	2	2.6	1.5	4.5	1	3	7	5.6	-

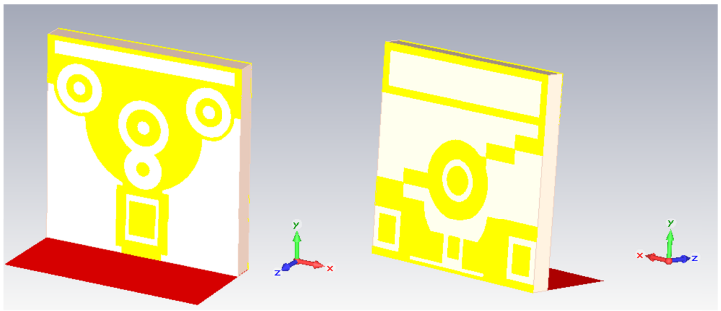

FIGURE 3. Prospective view of CubeSat antenna.

The antenna design includes front, side, and back views. The front view highlights circular and rectangular patch segments engineered for optimized radiation efficiency, while the side view reveals a substrate thickness of 1.5 mm. The back view features an advanced etched ground plane using circular and rectangular slots to improve bandwidth and impedance matching. This combined front-back optimization supports ultra-wideband (UWB) performance with enhanced radiation characteristics and efficiency, making it suitable for CubeSat and high-speed wireless communication applications. The antenna is designed on a Rogers RT/Duroid 5880 substrate, which has a relative permittivity (ε_r) of 2.2, a thickness of 1.5 mm, and a low loss tangent ($\tan\delta$) of 0.0009. These parameters are now explicitly mentioned, as they play a critical role in determining the antenna's impedance matching, radiation efficiency, and bandwidth performance. These material properties are critical for achieving wide bandwidth and high radiation efficiency, especially in the upper frequency ranges, where dielectric losses can significantly impact performance.

These carefully optimized values enable the antenna to support UWB performance. The integration of both front and back modifications in the design enhances impedance bandwidth and radiation efficiency.

3.2. Evolution of the Antenna

Figure 3 features a dual-layer configuration with a distinctive front and back structure, optimized for UWB performance. The front view showcases a semi-circular patch integrated with multiple slots and circular cut-outs, strategically dimensioned to enhance surface current distribution and impedance matching. The back view presents a complex ground plane with a combination of circular and rectangular etched slots, designed to support wideband and multi-resonance behavior.

Figure 4 illustrates the evolution of a planar antenna design from Stage 1 to Stage 4, showing a stepwise enhancement in geometry to achieve improved bandwidth and performance. In Stage 1, a basic circular patch is introduced as the primary radiator, serving as the foundational structure. Moving to Stage 2, the antenna is modified by incorporating symmetrical circular cut-outs on the upper side, which help in tuning resonant frequencies and slightly broadening the bandwidth. In Stage 3, a rectangular slot is added at the bottom portion of the radiator, improving impedance matching and enhancing the current distribution. Finally, in Stage 4, additional circular and rectangular slots are etched on the ground plane, resulting in significant improvement in impedance bandwidth, multi-resonance behavior, and overall antenna performance.

Figure 5 illustrates the progressive design development of the planar antenna from Stage 5 to Stage 8, with each step incorporating structural enhancements to optimize performance. In Stage 5, the antenna introduces an additional circular ring at the center of the radiator, which improves resonance characteristics and contributes to better bandwidth control. In Stage 6, small circular slots are added symmetrically around the structure, enabling multiple resonances and enhancing return loss

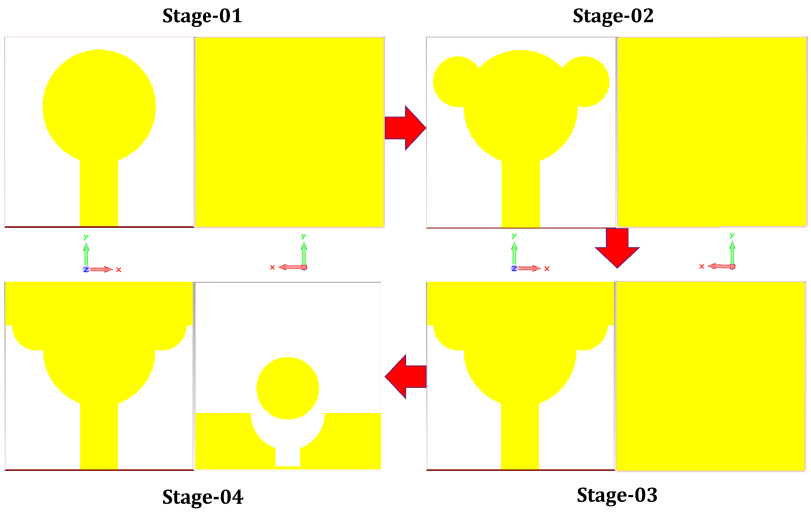

FIGURE 4. CubeSat antenna from stage 01-04.

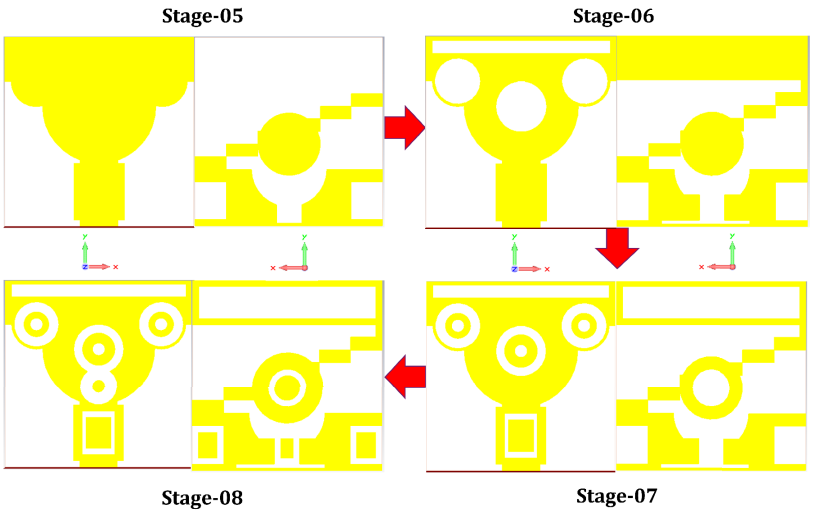

FIGURE 5. CubeSat antenna from stage 05-08.

characteristics. Stage 7 further refines the radiator by integrating a rectangular extension at the bottom and optimizing the slot configuration to improve current distribution and impedance matching. Finally, in Stage 8, detailed etching is introduced on the ground plane, combining circular and rectangular slots, resulting in a fully optimized structure with significantly widened impedance bandwidth and stable radiation performance across a broad frequency range.

This systematic design evolution highlights the impact of geometrical tuning on antenna efficiency and UWB operation.

4. RESULTS AND DISCUSSIONS

In Figure 6, S_{11} graph illustrates the return loss characteristics of the planar antenna across Stages 1 to 4, highlighting how successive design modifications enhance the antenna's impedance bandwidth. In Stage 1, the antenna begins resonating from 6 GHz to 12 GHz with a minimum S_{11} around 15 dB, indicating decent matching in the higher frequency range. With the modifications in Stage 2, the resonance shifts towards the lower band, expanding the bandwidth from 5.5 GHz to 12 GHz, showing improved performance. In Stage 3, significant changes to the structure allow the antenna to start resonating as low as 4 GHz, extending up to 10 GHz, which reflects better multi-resonant behavior and wider coverage. Finally, in Stage 4, the antenna achieves an optimized response with resonance ranging from 4.2 GHz to 12 GHz, maintaining S_{11} values below 10 dB across the band.

Figure 7 illustrates the progressive design evolution of a planar antenna from Stage 5 through Stage 8, with each stage introducing targeted structural modifications to enhance electromagnetic performance, specifically focusing on return loss (S_{11}), impedance bandwidth, and resonant characteristics. In Stage 5, the integration of a central circular ring into the radiator marks a foundational improvement, enabling a wide resonance bandwidth from 4.2 GHz to 12 GHz with perfect impedance matching. This design lays the groundwork for UWB functionality by optimizing resonance behavior and minimizing signal reflection. In Stage 6, the addition of symmetrically placed

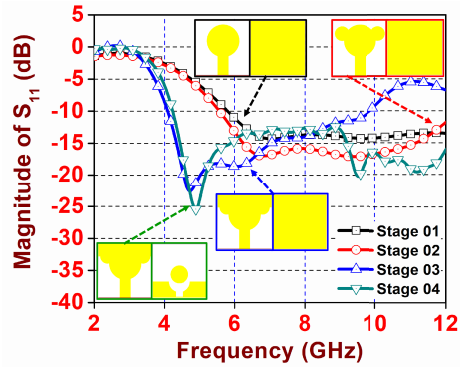

FIGURE 6. S_{11} from step-01 to step-04.

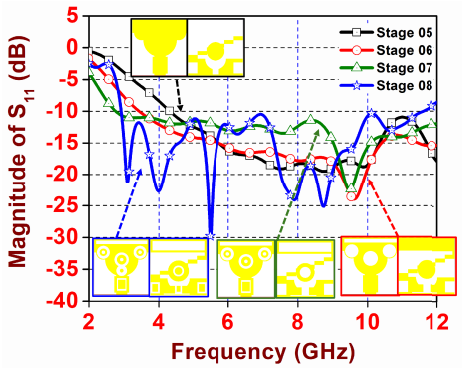

FIGURE 7. S_{11} from step-05 to step-08.

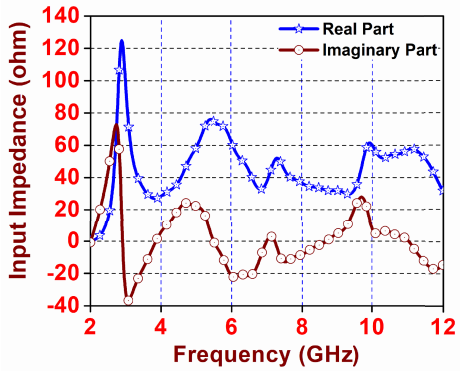

FIGURE 8. Input impedance curve.

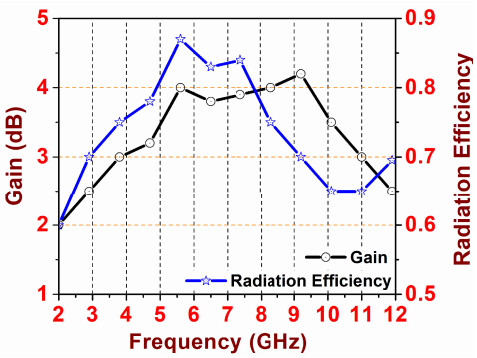

FIGURE 9. Simulated gain and efficiency curve.

small circular slots around the radiator enables multiple resonant modes and shifts the frequency response to a lower band, expanding the resonance range from 3.8 GHz to 12 GHz and further enhancing return loss performance.

Stage 7 continues this refinement by introducing a rectangular extension at the radiator's base and optimizing the slot configuration, which collectively improve current distribution and impedance matching. These changes result in an even broader resonance range, starting at 2.7 GHz and extending to 12 GHz, signaling a significant advancement in low-frequency performance. Finally, Stage 8 employs detailed etching on the ground plane featuring both circular and rectangular slots to produce a fully optimized antenna structure. This final configuration achieves a resonance range of 2.9 GHz to 11.6 GHz with an impedance bandwidth of approximately 120%, demonstrating superior UWB capability and stable radiation characteristics. The stepwise geometrical tuning throughout these stages underscores the critical role of structural design in achieving efficient and broadband antenna performance.

Figure 8 inputs impedance analysis of the planar antenna, as shown in the plots, and highlights significant improvements in impedance characteristics across the frequency range of interest. The real part of the impedance remains consistently close to the ideal 50-ohm line, particularly within the frequency band of approximately 2.9 GHz to 11.6 GHz. This indicates efficient impedance matching and minimal reflection losses throughout this UWB range. The real impedance is especially stable around key frequencies such as 3 GHz, 5 GHz, 7 GHz, and up to 11 GHz, demonstrating the antenna's capability to maintain near-optimal power transfer over a broad spectrum. These values confirm the antenna's suitability for broadband applications, with excellent matching characteristics that reduce signal loss and enhance overall efficiency.

In parallel, the imaginary part of the input impedance, which reflects the antenna's reactive behavior, stays close to zero ohms across the same wide frequency span, particularly from 2.9 GHz to 11.6 GHz. Notably, at frequencies like 3.5 GHz, 6 GHz, and 9 GHz, the imaginary impedance exhibits minimal deviation, indicating resonant conditions where the antenna is neither inductive nor capacitive. This low-reactance behavior across a wide range of frequencies ensures minimal reactive power and improved radiation efficiency. The combined behavior of both real and imaginary impedance parts over this range confirms that the antenna is finely tuned for UWB operation, offering both excellent impedance matching and stable performance.

The curves in Figure 9 illustrate the antenna's performance trends across the frequency range of 2 GHz to 14.6 GHz. The gain curve shows a gradual increase from 2 dBi at 2 GHz to a peak gain of 4.2 dBi at 9.2 GHz, representing the antenna's improved radiation directionality and effectiveness within the mid-band region. The curve maintains a relatively flat and stable profile between 3.8 GHz and 10.1 GHz, where the gain stays mostly above 3 dBi, indicating consistent radiation performance. After reaching its peak, the curve trends are downward beyond 10 GHz, reflecting a gradual drop in gain to around 2.7 dBi by 14.6 GHz. This behavior suggests that the antenna is best optimized for mid-frequency operation, with reduced effi-

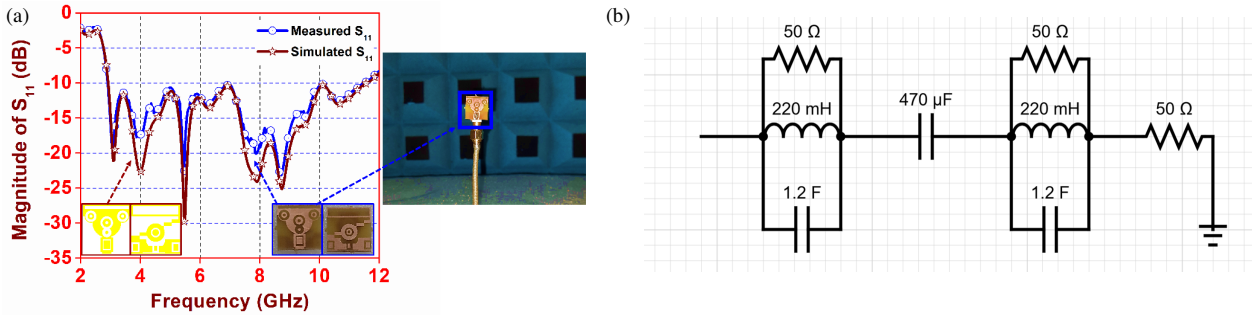

FIGURE 10. (a) Comparison of reflection coefficient (S_{11}). (b) Equivalent circuit model.

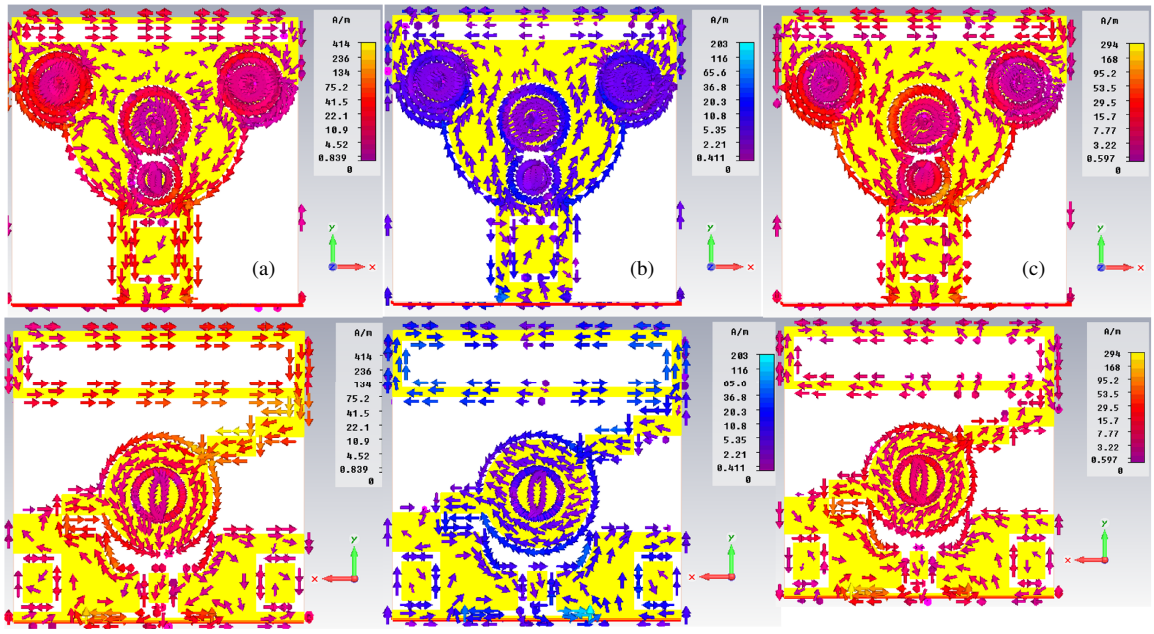

FIGURE 11. Simulated surface current distribution at (a) 3 GHz, (b) 6 GHz, (c) 9.2 GHz.

ciency at higher frequencies due to increased losses or reduced matching quality. The slight decline in radiation efficiency at higher frequencies can be attributed to increased dielectric and conductor losses. Despite the low loss tangent ($\tan\delta = 0.0009$) of the Rogers RT/Duroid 5880 substrate, material losses become more significant at higher frequencies due to increased electric field intensity and surface wave propagation. These factors contribute to the observed reduction in gain and must be considered when evaluating the antenna's upper-band performance.

The radiation efficiency curve similarly follows a bell-shaped trend. Starting at 60% efficiency at 2 GHz, and the curve rises sharply, reaching its maximum efficiency of 87% at 5.6 GHz. This peak marks the point of optimal electromagnetic performance, where the antenna effectively converts most input power into radiated energy. From there, the curve maintains good performance (above 75%) up to around 8.3 GHz, after which it gradually declines. By 10.1 GHz, the efficiency has decreased to 65% and continues to drop to around 58% at 14.6 GHz. The shape of the curve indicates that the antenna performs with high efficiency primarily in the mid-band region (4–8 GHz) and loses efficiency at both the low and high ends of the spectrum. Overall, the curves confirm that the antenna is well tuned for moderate gain and high radiation efficiency within a broad yet defined operating band. The antenna was realized on a Rogers RT/Duroid 5880 substrate with a thickness of 1.5 mm. The low loss tangent of 0.0009 and low dielectric constant ($\varepsilon_r = 2.2$) ensure minimal signal degradation and support efficient radiation over the antenna's wide operating bandwidth.

In Figure 10(a), S_{11} graph illustrates the performance of the fabricated antenna over a wide frequency range from 2.9 GHz to 11.6 GHz, where the reflection coefficient stays below -10 dB, indicating effective impedance matching and minimal power loss. The radiator achieves an impressive impedance bandwidth of approximately 120%, classifying it as an ultra-wideband (UWB) antenna. The antenna was fabricated using a chemical etching process to ensure precise and accurate patterning, and testing was conducted using a Vector Network Analyzer (VNA) inside an anechoic chamber to eliminate external electromagnetic interference. Simulated and measured S_{11} results are compared in the graph, showing strong correlation and validating the antenna design's reliability and consistency.

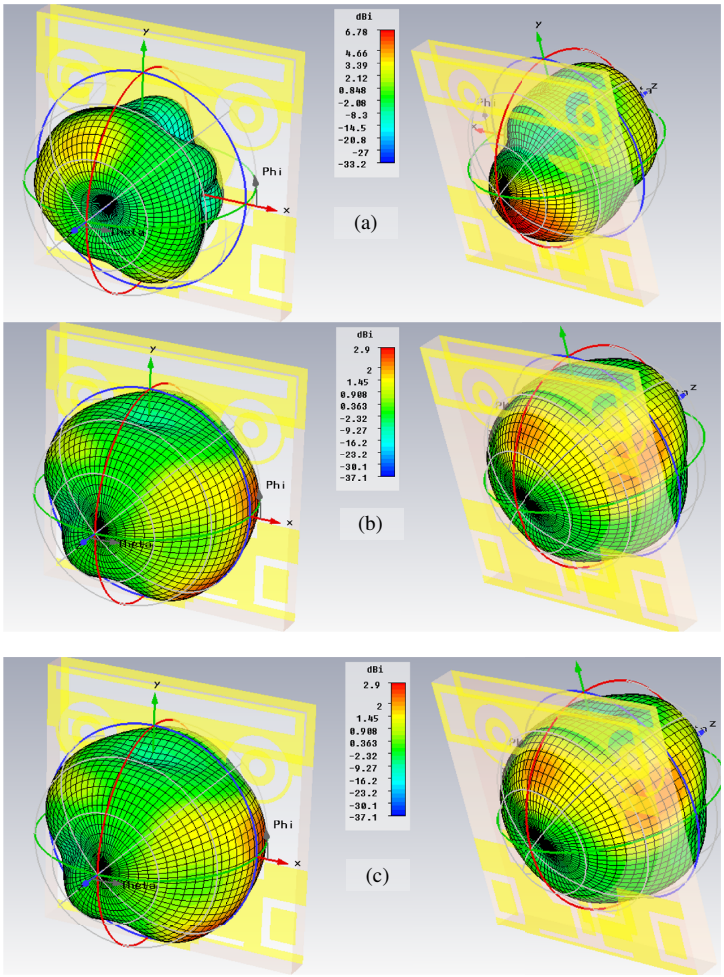

FIGURE 12. Radiation antenna lobe patterns, (a) 3 GHz, (b) 6 GHz, (c) 9 GHz.

To provide a deeper theoretical foundation for the chosen etching shape on the ground plane, an equivalent circuit model has been developed and is illustrated in Figure 10(b). This circuit model captures the dual-band characteristics of the antenna, with each resonant path represented by a parallel RLC tank circuit. Specifically, the resonant branches are tuned to operate at 5.5 GHz (Band-1) and 8 GHz (Band-2), with inductance and capacitance values of 220 mH and 1.2 F, respectively, selected to match the targeted resonant frequencies. The intermediate coupling capacitor (1.2 F) and terminating resistors (50 Ω) model the transmission path and impedance matching conditions.

The etched slots in the ground plane physically realize these frequency-selective behaviors. The shape and position of the etching influence the surface current distribution and create virtual LC paths that emulate the behavior of the RLC branches in the equivalent circuit. These slots introduce discontinuities and reactive elements that support the desired resonances, thereby validating the antenna's dual-band operation through a physical interpretation of the modeled circuit behavior.

This circuit-level analysis supports the phased optimization process and provides an electromagnetic interpretation for the structural modifications, particularly the ground plane etching. The model confirms that the selected geometry is not arbitrary but grounded in the equivalent circuit theory, reinforcing the persuasiveness and physical validity of the proposed design.

Figure 11(a) shows that the surface current distribution at 3 GHz shows a relatively smooth and widespread pattern, with current density primarily concentrated along specific edges and corners of the structure. This suggests that the structure operates near or slightly below its resonant frequency, resulting in less intense and more distributed surface currents. The current paths are well defined but not highly confined, indicating moderate energy coupling and radiation efficiency at this frequency.

In contrast, Figures 11(b) and (c) show that at 6 GHz and 9.2 GHz, the surface current becomes significantly more intense and localized. The current density is higher, and the distribution shows stronger confinement to certain regions of the structure, particularly around resonant elements or geometrical discontinuities. This concentrated current flow suggests that the structure resonates more efficiently at 6 GHz, leading to enhanced radiation and possibly higher gain. The sharpness and intensity of the current indicate that this frequency may align more closely with a designed resonant mode of the antenna or device.

Figure 12(a) shows 3 GHz, and 3D radiation lobe appears broad and less directive, indicating that the antenna radiates

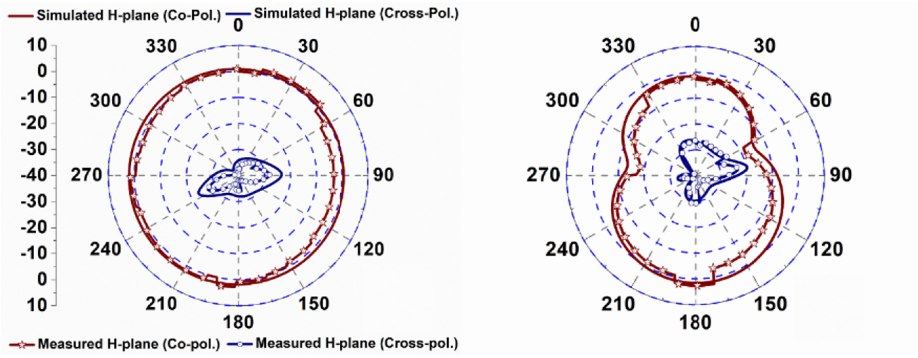

FIGURE 13. Co and cross polarizations at 5.5 GHz and 8 GHz.

TABLE 2. Comparison table.

Ref.	Band (GHz)	Electrical size (in λ)	Gain (dBi)	B/W (%)	(η) (%)
[2]	3.1–11	$0.20\lambda \times 0.25\lambda \times 0.015\lambda$	5.1	110%	89%
[3]	2–9	$0.33\lambda \times 0.22\lambda \times 0.1\lambda$	4.5	127%	62%
[6]	3.5–19	$0.23\lambda \times 0.23\lambda \times 0.015\lambda$	3.2	145%	81%
[7]	9.5–10.36	$0.6\lambda \times 0.06\lambda \times 0.004\lambda$	4.4	$< 1\%$	NA
[8]	2.9–16	$0.33\lambda \times 0.24\lambda \times 0.014\lambda$	5.2	139%	87%
[9]	2.8–12	$0.18\lambda \times 0.14\lambda \times 0.15\lambda$	2.79	122%	72%
[10]	2.7–7.3	$0.32\lambda \times 0.2\lambda \times 0.014\lambda$	2.3	108%	78.3%
[11]	42.48–45.2	$0.10\lambda \times 0.12\lambda \times 0.02\lambda$	4.3	87%	NA
Presented	**2.9–11.6**	$\mathbf{0.14\lambda \times 0.14\lambda \times 0.014\lambda}$	**4.2**	**120%**	**87%**

energy over a wider angular region. The shape of the lobe is more spherical or omnidirectional, suggesting low directivity and gain. This pattern is typical for antennas operating below or near their fundamental resonant frequency, where energy is not tightly focused in one direction. The radiation is likely suitable for applications requiring wide coverage rather than long-range or directional communication.

Figures 12(b) and (c) show radiation lobe patterns at 6 GHz and 9 GHz, and the radiation lobes become increasingly focused and directive. At 6 GHz, the lobe shows noticeable narrowing, forming a more defined main beam, which suggests improved antenna directivity and higher gain. By 9 GHz, the radiation pattern becomes even more concentrated in a specific direction, with a sharper and narrower beam, characteristic of higher frequency operation where the antenna supports higher-order resonant modes. It indicates that the antenna becomes more efficient and suitable for targeted communication or radar applications at these higher frequencies.

Figure 13 illustrates the co-polarization and cross-polarization radiation patterns at 5.5 GHz and 8 GHz, plotted in two principal planes for clarity. The H-plane corresponds to the XoZ plane at 0°, while the E-plane is taken along the YoZ plane at 90°. In the H-plane, the plots display a consistent circular radiation pattern, highlighting uniform power distribution across all azimuthal directions, an essential feature for achieving omnidirectional coverage. In contrast, the E-plane exhibits a classic bidirectional or figure-eight pattern, with strong lobes extending in opposite directions along the vertical axis. This combination ensures broad horizontal reach and focused vertical performance. Additionally, the dominance of co-polarized components over cross-polarized ones in both planes reflects good radiation efficiency and polarization purity. The close alignment between simulated and measured results further supports the reliability of the design. Collectively, these characteristics indicate that the antenna is well suited for applications such as CubeSat and ultra-wideband communications, where stable omnidirectional and bidirectional radiation behaviors are critical.

Table 2 compares the proposed antenna with previously documented designs. After evaluating several parameters, our analysis indicates that the proposed design is smaller in size and exhibits improved characteristics compared to those of previously reported antennas.

5. CONCLUSION

The designed planar antenna exhibits outstanding ultra-wideband (UWB) capabilities, achieved through careful geometric refinement and structural design improvements. It supports a broad impedance bandwidth ranging from 2.9 GHz to 11.6 GHz. The antenna maintains a compact footprint of 15 mm × 15 mm, which corresponds to an electrical size of approximately $0.14\lambda \times 0.14\lambda \times 0.014\lambda$ at a central operating frequency of 8.7 GHz and also supports integration into space-constrained RF systems. With a peak gain of 4.2 dBi and radiation efficiency up to 87%, the antenna ensures stable far-field characteristics and high performance across the

band. The innovative design featuring front-side radiators and a modified ground plane enhances impedance matching and bandwidth, making it ideal for tactical communications, electronic warfare, and CubeSat applications. Covering critical frequency bands such as S-, C-, X-, and portions of the Ku-band, the antenna is well suited for high-throughput, low-SWaP satellite systems requiring reliable telemetry and robust signal integrity.

REFERENCES

[1] Mishra, B., R. K. Verma, R. K. Singh, *et al.*, "A review on microstrip patch antenna parameters of different geometry and bandwidth enhancement techniques," *International Journal of Microwave and Wireless Technologies*, Vol. 14, No. 5, 652–673, 2022.

[2] Khidre, A., K.-F. Lee, A. Z. Elsherbeni, and F. Yang, "Wide band dual-beam U-slot microstrip antenna," *IEEE Transactions on Antennas and Propagation*, Vol. 61, No. 3, 1415–1418, 2013.

[3] Shagar, A. C. and S. D. Wahidabanu, "Novel wideband slot antenna having notch-band function for 2.4 GHz WLAN and UWB applications," *International Journal of Microwave and Wireless Technologies*, Vol. 3, No. 4, 451–458, 2011.

[4] Tiwari, A., D. Yadav, P. Sharma, and M. V. Yadav, "Design of wide notched-band circular monopole ultra-wideband reconfigurable antenna using PIN diodes switches," *Progress In Electromagnetics Research C*, Vol. 139, 107–118, 2023.

[5] Kurniawan, A. and S. Mukhlishin, "Wideband antenna design and fabrication for modern wireless communications systems," *Procedia Technology*, Vol. 11, 348–353, 2013.

[6] Ghosh, A., S. K. Ghosh, D. Ghosh, and S. Chattopadhyay, "Improved polarization purity for circular microstrip antenna with defected patch surface," *International Journal of Microwave and Wireless Technologies*, Vol. 8, No. 1, 89–94, 2016.

[7] Baudha, S. and M. V. Yadav, "A compact ultra-wide band planar antenna with corrugated ladder ground plane for multiple applications," *Microwave and Optical Technology Letters*, Vol. 61, No. 5, 1341–1348, 2019.

[8] Abdelraheem, A. M. and M. A. Abdalla, "Compact curved half circular disc-monopole UWB antenna," *International Journal of Microwave and Wireless Technologies*, Vol. 8, No. 2, 283–290, 2016.

[9] Baudha, S., S. Gupta, and M. V. Yadav, "Parasitic rectangular patch antenna with variable shape ground plane for satellite and defence communication," in *2019 URSI Asia-Pacific Radio Science Conference (AP-RASC)*, 1–4, New Delhi, India, 2019.

[10] Awad, N. M. and M. K. Abdelazeez, "Multislot microstrip antenna for ultra-wide band applications," *Journal of King Saud University — Engineering Sciences*, Vol. 30, No. 1, 38–45, 2018.

[11] Yadav, M. V. and S. Baudha, "A miniaturized printed antenna with extended circular patch and partial ground plane for UWB applications," *Wireless Personal Communications*, Vol. 116, No. 1, 311–323, 2021.

[12] Deshmukh, A. A., D. Singh, P. Zaveri, M. Gala, and K. P. Ray, "Broadband slot cut rectangular microstrip antenna," *Procedia Computer Science*, Vol. 93, 53–59, 2016.

[13] Hota, S., M. V. Yadav, S. Baudha, and B. B. Mangaraj, "Miniaturized planar ultra-wideband patch antenna with semi-circular slot partial ground plane," in *2019 IEEE Indian Conference on Antennas and Propogation (InCAP)*, 1–4, Ahmedabad, India, 2019.

[14] Baudha, S. and M. V. Yadav, "A novel design of a planar antenna with modified patch and defective ground plane for ultra-wideband applications," *Microwave and Optical Technology Letters*, Vol. 61, No. 5, 1320–1327, 2019.

[15] Baudha, S., H. Garg, and M. V. Yadav, "Dumbbell shaped microstrip broadband antenna," *Journal of Microwaves, Optoelectronics and Electromagnetic Applications*, Vol. 18, 33–42, 2019.

[16] Yadav, M. V., S. V. Yadav, T. Ali, S. K. K. Dash, N. T. Hegde, and V. G. Nair, "A cutting-edge S/C/X band antenna for 5G and beyond application," *AIP Advances*, Vol. 13, No. 10, 105123, 2023.

[17] Hota, S., S. Baudha, B. B. Mangaraj, and M. V. Yadav, "A compact, ultrawide band planar antenna with modified circular patch and a defective ground plane for multiple applications," *Microwave and Optical Technology Letters*, Vol. 61, No. 9, 2088–2097, 2019.

[18] Mazinani, S. M. and H. R. Hassani, "A novel broadband plate-loaded planar monopole antenna," *IEEE Antennas and Wireless Propagation Letters*, Vol. 8, 1123–1126, 2009.

[19] Kim, G.-H. and T.-Y. Yun, "Compact ultrawideband monopole antenna with an inverted-L-shaped coupled strip," *IEEE Antennas and Wireless Propagation Letters*, Vol. 12, 1291–1294, 2013.

[20] Yadav, S. V., M. V. Yadav, T. Ali, S. K. K. Dash, N. T. Hegde, and V. G. Nair, "A circular compact ultra-wideband antenna for 5G microwave applications," *TELKOMNIKA (Telecommunication Computing Electronics and Control)*, Vol. 22, No. 3, 556–566, 2024.

[21] Gupta, R., M. V. Yadav, and S. V. Yadav, "TL-shaped circular parasitic compact planar antenna for 5G microwave applications," in *International Conference on Electrical and Electronics Engineering*, 507–515, Springer Nature Singapore, Singapore, 2023.

[22] Sethi, W. T., S. H. Kiani, M. E. Munir, D. A. Sehrai, H. S. Savci, and D. Awan, "Pattern diversity based four-element dual-band MIMO patch antenna for 5G mmWave communication networks," *Journal of Infrared, Millimeter, and Terahertz Waves*, Vol. 45, No. 5, 521–537, 2024.

[23] Munir, M. E., M. M. Nasralla, and M. A. Esmail, "Four port tri-circular ring MIMO antenna with wide-band characteristics for future 5G and mmWave applications," *Heliyon*, Vol. 10, No. 8, e28714, 2024.

[24] Munir, M. E., M. M. Nasralla, and H. Farman, "Design and development of super-compact millimeter wave antenna for future 5G vehicular applications," in *2024 IEEE 100th Vehicular Technology Conference (VTC2024-Fall)*, 1–8, Washington, DC, USA, 2024.

[25] Kukreja, J., D. K. Choudhary, and R. K. Chaudhary, "CPW fed miniaturized dual-band short-ended metamaterial antenna using modified split-ring resonator for wireless application," *International Journal of RF and Microwave Computer-Aided Engineering*, Vol. 27, No. 8, e21123, 2017.

[26] Kukreja, J., D. K. Choudhary, and R. K. Chaudhary, "A short-ended compact metastructure antenna with interdigital capacitor and U-shaped strip," *Wireless Personal Communications*, Vol. 108, 2149–2158, 2019.

[27] Constantine, A. B., *Antenna Theory: Analysis and Design*, 3rd ed., Wiley-Interscience, 2005.

[28] Pozar, D. M., *Microwave Engineering: Theory and Techniques*, 3rd ed., John Wiley & Sons, 2005.

[29] Mathur, V. and M. Gupta, "Comparison of performance characteristics of rectangular, square and hexagonal microstrip patch antennas," in *Proceedings of 3rd International Conference on Reliability, Infocom Technologies and Optimization*, 1–6, Noida,

India, 2014.

[30] Basu, S., A. Srivastava, and A. Goswami, "Dual frequency hexagonal microstrip patch antenna," *International Journal of Scientific and Research Publications*, Vol. 3, No. 11, 1–9, 2013.

[31] Kushwaha, N. and R. Kumar, "Design of slotted ground hexagonal microstrip patch antenna and gain improvement with FSS screen," *Progress In Electromagnetics Research B*, Vol. 51, 177–199, 2013.

[32] Cao, T., X. Zhang, W. Dong, L. Lu, X. Zhou, X. Zhuang, J. Deng, X. Cheng, G. Li, and R. E. Simpson, "Tuneable thermal emission using chalcogenide metasurface," *Advanced Optical Materials*, Vol. 6, No. 16, 1800169, 2018.

[33] Cao, T., G. Zheng, S. Wang, and C. Wei, "Ultrafast beam steering using gradient Au-$Ge_2Sb_2Te_5$-Au plasmonic resonators," *Optics Express*, Vol. 23, No. 14, 18 029–18 039, 2015.

[34] Soni, G. K., D. Yadav, A. Kumar, C. Sharma, and M. V. Yadav, "Flexible ring slot antenna for optimized 5G performance in N77 and N78 frequency bands for wearable applications," *Progress In Electromagnetics Research C*, Vol. 150, 47–55, 2024.

[35] Tiwari, A., D. Yadav, P. Sharma, and M. V. Yadav, "Design of wide notched-band circular monopole ultra-wideband reconfigurable antenna using PIN diodes switches," *Progress In Electromagnetics Research C*, Vol. 139, 107–118, 2023.